Laser Photodissociation Dynamics of Thionyl Chloride: Concerted and Stepwise Cleavage of S–Cl Bonds

Hongxin Wang, Xirong Chen, and Brad R. Weiner*

Department of Chemistry and Chemical Physics Program, University of Puerto Rico, Box 23346 UPR Station, Río Piedras, Puerto Rico 00931

Received: June 22, 1993; In Final Form: August 17, 1993®

The photodissociation of thionyl chloride (Cl_2SO) is of interest as a model system to study three-body fragmentation processes, which can occur either in concert or stepwise. The photodissociation of this tetratomic molecule at 193 and 248 nm has been studied by laser induced fluorescence spectroscopy of the nascent SO fragment on the $B^3\Sigma^- - X^3\Sigma^-$ transition in the region of 237–295 nm. Photolysis of Cl_2SO at 193 nm leads to an inverted vibrational distribution for the nascent $SO(X^3\Sigma^-)$ with a population maximum at $v'' = 2$. The quantum yield, $\Phi_{SO(X)}^{193\,nm} = 0.73 \pm 0.10$, has been measured by comparison of the $SO(X^3\Sigma^-)$ produced from SO_2. The results indicate a concerted three-body fragmentation mechanism as the primary dissociation channel. A Franck–Condon/golden rule model elucidates the geometry prior to the fragmentation and suggests a direct dissociation mechanism. The rotational- and spin-state distributions have been measured from the rovibronically resolved spectra to support our model of the detailed dissociation mechanism. At 248 nm, the nascent vibrational distribution was found to be bimodal. The vibrational state population distribution in $v'' = 0$–2, which accounts for most (~94%) of the nascent $SO(X^3\Sigma^-)$ population, was found to be thermal ($T_{vib} = 1000 \pm 200$ K), suggesting a stepwise fragmentation process. About 6% of the nascent SO population has been observed in other vibrational levels ($v'' = 3$–7) and most likely originates from the molecular elimination of Cl_2 from Cl_2SO.

Introduction

Real time descriptions of chemical processes have drawn a great deal of attention recently in dynamical studies of various chemical reactions, particularly in photodissociation reactions.[1] Photodissociation of molecules can be separated, in principle, into two major processes.[2] The first step is the electronic excitation of the parent molecule through the absorption of a photon, in which the initial conditions for the nuclear motion in the excited electronic state are defined.[2] The second step refers to the spontaneous decay of the parent molecule in the excited state into the nascent products and is known as the final state interaction.[2] For a photodissociation process producing three fragments, the concepts of concertedness and/or synchronicity need to be considered. A stepwise reaction is defined as one which occurs in two kinetically distinct steps via a long-lived intermediate, while a concerted reaction is one which proceeds in a single kinetic step.[3] Some concerted reactions can be synchronous, *i.e.*, where all the bond-breaking events take place with exactly the same rate and in phase.[4] In a multiple bond-breaking photodissociative event, such as ABCD → AB + C + D, if the bonds in the parent molecule fragment within a given time, the process is considered to be in concert, otherwise it is stepwise.[5] This defined time can be determined for the molecule itself.[6] For the limiting case of a concerted dissociation, where ABCD fragments into AB + C + D synchronously, the spatial angular distribution of the fragments would be narrow. In the opposite case, a stepwise dissociation, where D was to dissociate first while ABC rotates freely about its center of mass prior to its dissociation, an isotropic spatial angular distribution of fragment C would result. Therefore, the rotational period of the ABC intermediate provides an accepted criterion for distinguishing between a concerted and a stepwise process.[5] This can be elucidated experimentally by measuring the spatial anisotropy of the fragments.

The tetratomic molecule, thionyl chloride (Cl_2SO), offers an excellent test case for three-fragment photodissociation studies.[6–8] Several previous studies have examined various aspects of the electronic structure of and photodissociation dynamics of Cl_2SO.[6–9] The ground-state molecular structure has been determined by Suzuki *et al.* by using microwave spectroscopy.[9] The UV absorption spectrum of Cl_2SO shows an origin near 300 nm with two absorption maxima at 194 nm ($\sigma = 1.3 \times 10^{-17}$ cm^2) and 244 nm ($\sigma = 7.1 \times 10^{-18}$ cm^2).[10] These absorption maxima have been assigned previously to $n_{Cl} \rightarrow \sigma_{S-Cl}^*$ and $n_S \rightarrow \sigma_{S-Cl}^*$ type electronic transitions, respectively, by comparison with molecular orbital calculations.[6,11] The vacuum UV absorption spectrum and photochemistry of Cl_2SO between 116 and 135 nm has also been studied by Okabe.[12] Flash photolysis of this tetratomic molecule was first investigated in the far UV region by Donovan *et al.* by using transient absorption spectroscopy.[13] Kawasaki *et al.* used photofragment time-of-flight spectroscopy to investigate the excimer laser photodissociation process of thionyl chloride.[6] They found evidence for two distinct SO-producing channels in the 193-nm photolysis of Cl_2SO: three-body fragmentation to give two Cl atoms and molecular elimination of Cl_2. Emission spectra in the region of 220–340 were observed and assigned to $SO(B \rightarrow X)$ and $Cl_2(B \rightarrow X)$ transitions following the 248-nm irradiation of Cl_2SO.[6] These spectra most likely arise from secondary 248-nm excitation of the nascent SO and Cl_2 fragments. No information about SOCl was reported. Baum *et al.* have studied the photodissociation of Cl_2SO at both 193 and 248 nm, once again by using photofragment time-of-flight translational spectroscopy and probing at $m/e = 35$, 48, 70, and 83 corresponding to Cl, SO, Cl_2, and SOCl, respectively.[8] Their experiments lead to the branching ratios shown in Table I for the ultraviolet photodissociation.[8] A schematic energy diagram based on the previously reported data[8,14] was developed and is shown as Figure 1. In the photodissociation of Cl_2SO at 248 nm, channels (1) and (2), with a branching ratio of 30:1, are the only operative reactions.[8] In the molecular elimination channel, the nascent products of $SO(b^1\Sigma^+)$ and $SO(X^3\Sigma^-)$ were found to have a ratio of 9:1. No three-body dissociation (3) has been observed,[8] even though it is energetically feasible following absorption of a 248-nm photon (115 kcal/mol).[8,14] An energy barrier may exist to

* Author to whom correspondence should be addressed.
® Abstract published in *Advance ACS Abstracts*, October 1, 1993.

0022-3654/93/2097-12260$04.00/0

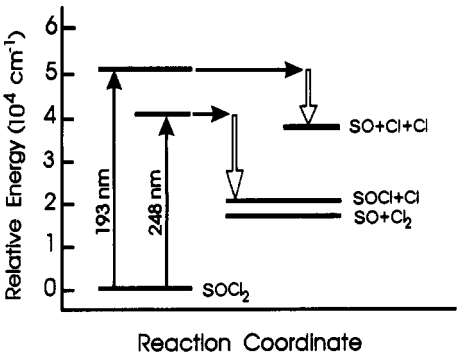

Figure 1. A schematic energy diagram for the photodissociation of Cl_2SO at 193 and 248 nm.

TABLE I

$Cl_2SO + h\nu$	ΔH_{rxn} (kcal/mol)	production yield[8] at 248 nm (%)	at 193 nm (%)	
→ SOCl + Cl	57.3	96.5	17	(1)
→ SO + Cl_2	51.3	3.5	3	(2)
→ SO + Cl + Cl	108.5		80	(3)

prevent such a photochemical process from proceeding directly. At 193 nm, Baum *et al.* found that about 17% of the photoactivated Cl_2SO molecules undergo single bond fission (1) and less than 3% proceed via the molecular elimination channel (2). Following the homolytic cleavage (1) there may be further fragmentation of SOCl into SO and Cl, either through a unimolecular decay or via a secondary photodissociation. Both of these possibilities were ruled out by experiments of Baum *et al.*[8] The possibility of further fragmentation of Cl_2 into two Cl atoms was eliminated as well.[8] The authors thus concluded that the remaining 80% of photoactivated Cl_2SO undergoes a three-body dissociation (3).

Hirota and co-workers employed 193-nm photolysis of Cl_2SO as a source for infrared diode laser absorption studies of SO($a^1\Delta$), which lies 18 kcal/mol above the ground-state SO($X^3\Sigma^-$).[15] They found a branching ratio of 1:4 for SO($a^1\Delta$) to SO($X^3\Sigma^-$). The SO($a^1\Delta$) radicals were produced with significant vibrational (up to $v'' = 5$) and rotational (up to $N'' = 40$) excitation. Stuart *et al.* have investigated the saturation of SO(A–X) excitation following the photodissociation of Cl_2SO with both narrow and broad band KrF laser emission.[16] They measured SO(A–X) absorption saturation fluence and determined the efficiency of SO($A^3\Pi$) excitation with possible applications to an ultraviolet energy storage laser. No photodissociation mechanism of Cl_2SO was discussed in their report.

Investigation of the energy disposal into the rovibronic states of the nascent fragment or fragments from the photodissociation of molecules can reveal the detailed dissociation mechanisms.[7,17] In the case of multiple bond breaking in a polyatomic molecule, this can help distinguish whether the process occurs in a concerted or in a stepwise manner.[7,17] While the previous experiments have addressed the branching ratio from Cl_2SO photolysis based on photofragment translational spectroscopy, the internal state distributions of the nascent fragments are almost unknown. A nascent vibrational distribution of SO($X^3\Sigma^-, v''$) from the photolysis of Cl_2SO at 193 nm was recently described by us in a letter.[7] However, no rotational-state distributions of the nascent SO($X^3\Sigma^-$) have been previously reported, and no detailed dissociation mechanism, related to the energy disposal into the internal states of the nascent fragments, has been addressed. We report here our measurements on the nascent vibrational-, rotational-, and spin-state distributions and the quantum yield of the nascent SO($X^3\Sigma^-$) following excimer laser photolysis of Cl_2SO at 193 and 248 nm. The SO($X^3\Sigma^-, v'' = 0$–7) was observed directly by using laser induced fluorescence (LIF) spectroscopy on the $B^3\Sigma^-$–$X^3\Sigma^-$ transition. These data provide valuable insight toward a more complete understanding of the 193 and 248 nm photodissociation of thionyl chloride.

Experimental Section

The experiments were performed in a standard laser pump-probe apparatus, which has been described in detail previously.[7,18] Briefly, the purified sample, either neat or in buffer gas, was flowed through a glass four-way cross which serves as the reaction chamber. The glass cross is extended with glass arms at each side, along the laser axis, to reduce the scattered light. Gas inlets are located on the extension arms, while the outlet to the vacuum is located near the reaction zone. Heterogeneous decomposition of Cl_2SO was minimized by using only glass, polyethylene, and stainless steel components for the reaction cell and the inlet system.[8] The system was passivated for about 0.5 h before the experiment. The reaction cell was pumped to a vacuum of 10^{-3} Torr by a mechanical pump, and the pressure of the chamber was measured at the exit by a capacitance manometer.

In our experiments, the reactant vapor, Cl_2SO, was photolyzed with either the 193-nm (25–30 mJ/cm^2) or 248-nm output (60–70 mJ/cm^2) of an excimer laser (Lambda Physik LPX205i), operating on the ArF and KrF transitions, respectively. Nascent SO radicals were monitored by laser induced fluorescence (LIF) spectroscopy on the $B^3\Sigma^-$–$X^3\Sigma^-$ transition in the 237–295-nm region of the spectrum. The probe laser in this region was generated by frequency doubling (β-BaB_2O_4 crystal) the output of a Lambda Physik FL3002 tunable dye laser (dyes used: Coumarin 460, Coumarin 480, Coumarin 503, and Coumarin 540A), which was pumped by a Lambda Physik LPX205i excimer laser operated at 308 nm. The two lasers were collinearly counterpropagated along the extension arm axis to maximize the overlap region in the center of the reaction cell. Laser induced fluorescence was viewed at 90° relative to the laser beam axis by a high gain photomultiplier tube through longpass filters (Schott WG295, WG305). The output of the photomultiplier tube was processed and averaged by a gated integrator (Stanford Research System (SRS); Model SR250), digitized (SRS; model 245) and sent to a personal computer for screen display, data storage, and analysis. The delay time between the two lasers was controlled with a digital delay pulse generator (SRS; model DG535) and was fixed between 300–2000 ns, while the frequency-doubled output of the dye laser was scanned to collect the total fluorescence signal to obtain a nascent LIF excitation spectrum. The photolysis laser was operated at a repetition rate of 40 Hz, and each data point represents the average of 10 laser shots. The LIF intensity was found to be linear as a function of dye laser power, and the signals, taken over a large wavelength region, were normalized to the dye laser power.

Commercial thionyl chloride (Fluka, ≥99.5%) was purified by doubly distilling under vacuum which leads to a colorless liquid. The sample was prepared on a vacuum line containing only glass and stainless steel. To remove possible SO_2 impurities,[6,8] the sample was continuously pumped at 0 °C for several minutes before a day's experiments. The residual SO_2 in a gas-phase sample during the experiments was found to be less than 1% by using laser induced fluorescence monitoring of SO_2. Sulfur dioxide (Air Products, 99.8%) was used directly as supplied, as a calibrant and as an actinometer in the quantum yield experiments. Helium (General Gases, 99.9%) was used directly, without further purification.

Results

1. Vibrational State Distribution of Nascent SO($X^3\Sigma^-$). The vibrational-state population distributions of the nascent SO($X^3\Sigma$, v') resulting from the photodissociation of Cl_2SO at 193 and 248 nm have been determined by using LIF excitation spectroscopy on the SO($B^3\Sigma^-$–$X^3\Sigma^-$) transition in the region of 237–295 nm (see Figure 2). The vibrational bands terminating on the $v' = 1$ level of the B state, ($1, v'' = 0$–7), were used to determine the

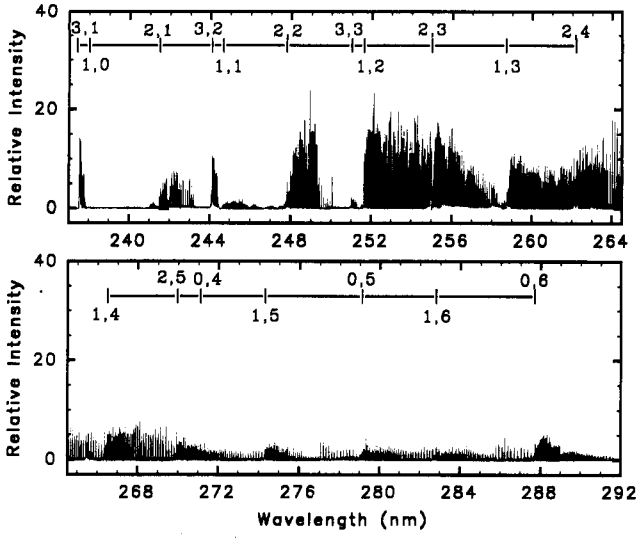

Figure 2. LIF spectrum of nascent SO($X^3\Sigma^-$–$B^3\Sigma^-$) following the 193-nm photolysis of 0.020 Torr of Cl_2SO. The delay between the photolysis and probe laser was 400 ns. The origins of the vibrational bands have been assigned from ref 19.

nascent vibrational population. Assignment of these bands was accomplished by using Colin's spectroscopic data.[19] The measured integrated band areas under this spectrum were analyzed and normalized for Franck–Condon factors of the SO($B^3\Sigma^-$–$X^3\Sigma^-$) transition to obtain the relative vibrational-state populations of SO($X^3\Sigma^-$, v'' = 0–7).[20] While some discrepancy about the accuracy of the Franck–Condon factors in the SO($B^3\Sigma^-$–$X^3\Sigma^-$) transition exists for higher vibrational levels ($v' > 6$) of the upper electronic state, the calculations for $v' \leq 6$ have been shown to be reliable through agreement with values obtained from Morse potential curves.[20] In the 193-nm photodissociation of thionyl chloride, the LIF excitation spectrum was obtained under collision-free conditions (0.020 Torr Cl_2SO, 400 ns probe delay). For the 248-nm photodissociation experiments, a 1-μs delay time was the minimum possible due to the strong scattered light and secondary fluorescence from the pump laser. Helium (*ca.* 1 Torr) was blown onto the reaction cell windows to minimize deposit buildup that would subsequently reduce the amount of UV laser light passing into the cell. Consequently, each SO radical undergoes *ca.* 10 gas-phase collisions prior to detection. While these collisions may affect the nascent rotational-state distributions (see below), the vibrational-state population distributions are virtually unperturbed. This result has been confirmed by recent studies of the vibrational relaxation of sulfur monoxide in this laboratory, which shows approximately 10^4 gas-phase collisions in helium are required to completely thermalize the SO vibrational-state distribution.[21]

In the case of 193-nm photolysis, the vibrational-state distribution of the nascent SO($X^3\Sigma^-$) has previously been reported by this laboratory.[7] In those experiments, the nascent SO($X^3\Sigma^-$) photofragment was probed by LIF spectroscopy on the $A^3\Pi$–$X^3\Sigma^-$ electronic transition.[7] In the present experiments, the B–X transition as opposed to the A–X transition was monitored to improve our sensitivity for the higher vibrational levels due to the larger Franck–Condon factors.[20] The nascent vibrational-state population of the SO($X^3\Sigma^-$) following the 193-nm photolysis (see Table II and Figure 3) has been observed up to $v'' = 6$, and the distribution has been found to be inverted with a population maximum of 35 ± 6% at $v'' = 2$. However, the nascent population may peak in the adjacent state of $v'' = 1$ (30 ± 8%). This observation is different from the result previously reported by Chen *et al.*,[7] where an inverted nascent vibrational distribution with a population maximum at $v'' = 3$ was observed. The discrepancy in the measurements might be due to the weakness of the A–X transition and the spectral overlap between the A–X and B–X transitions. It may also have resulted from decomposition and/or SO_2 impurities in the Cl_2SO sample in the previous study.

TABLE II: Experimentally Obtained Vibrational State Distributions of the Nascent SO($X^3\Sigma^-$) Following the Photodissociation of Cl_2SO at 193 and 248 nm

	relative population (%)	
v''	at 193 nm	at 248 nm
0	≤5	71 ± 9
1	30 ± 8	20 ± 5
2	35 ± 6	3 ± 1
3	20 ± 4	0.5 ± 0.2
4	7 ± 1	2 ± 0.3
5	2 ± 0.5	2.5 ± 0.3
6	1 ± 0.2	0.8 ± 0.2
7	(0)[a]	0.2 ± 0.1

[a] No nascent population in the SO($X^3\Sigma^-$, $v'' = 7$) state has been measured following the photolysis of Cl_2SO at 193 nm

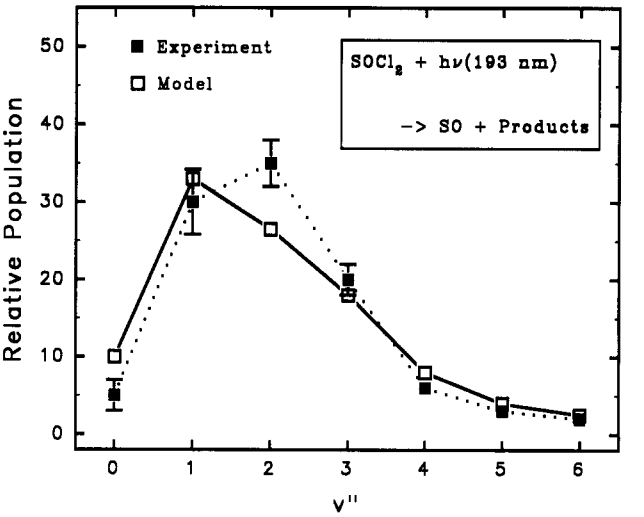

Figure 3. Vibrational state distribution of the nascent SO($X^3\Sigma^-$, v'') fragment following the photolysis of Cl_2SO at 193 nm. The filled symbols, ■, represents the experimentally observed distribution, while the open symbol, □, stands for a calculated distribution by using a Franck–Condon/golden rule model (see text).

Following the 248-nm UV irradiation of Cl_2SO, a bimodal vibrational-state distribution has been found for the nascent SO($X^3\Sigma^-$) fragment, as shown in Table II and Figure 4. In this case, the majority of the nascent SO($X^3\Sigma^-$) population (94%) was found in $v'' = 0$–2, while the remaining 6% populated $v'' = 3$–7 with a second peak at $v'' = 5$. The signal intensity in several vibrational states, *e.g.*, (1,1) and (1,5) transition band, have been measured as a function of the photolysis laser fluence and, in all cases, was found to be linear, suggesting a single photon process in the production of all the nascent SO($X^3\Sigma^-$) fragments. The nascent population in the first three vibrational levels ($v'' = 0$–2) of the SO($X^3\Sigma^-$) radicals can be fit to a Boltzmann distribution

$$P(v'') \propto \exp[-E_{vib}/K_B T_{vib}] \quad (4)$$

where E_{vib} is the vibrational energy of the corresponding levels. The vibrational temperature, T_{vib}, was found to be 1000 ± 200 K.

2. Rotational-State Distribution of Nascent SO($X^3\Sigma^-$). The SO($B^3\Sigma^-$–$X^3\Sigma^-$) LIF spectra, (*e.g.*, Figure 5 and 6), have been used for the measurement of rotational-state population distributions following the 193-nm photolysis of Cl_2SO. Only six branches, namely P_{11}, P_{22}, P_{33}, R_{11}, R_{22}, and R_{33}, are strongly allowed for the SO(B–X) transition.[19,22,23] P_{22} and R_{22} were resolved for $N > 10$ and 15, respectively (*e.g.*, see Figure 6), for our maximum spectral resolution (*ca.* 0.25 cm^{-1}). The assignment of these partially resolved spectra was made by calculating the

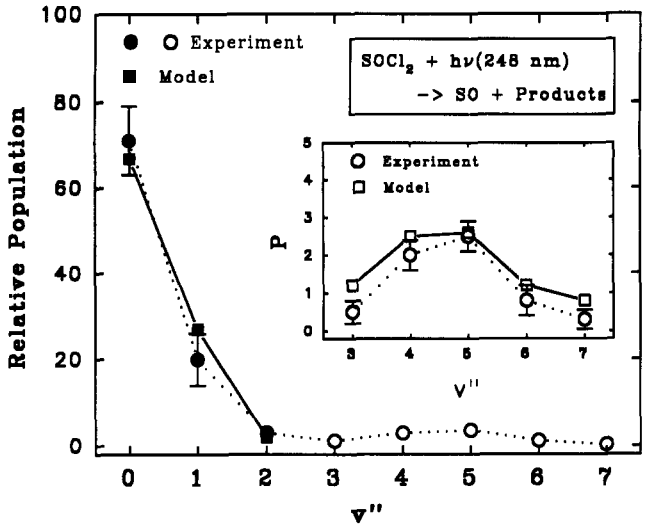

Figure 4. Vibrational state distribution of the nascent $SO(X^3\Sigma^-, v'')$ fragment following the photolysis of Cl_2SO at 248 nm. The round symbols, ● and ○, represent the experimental measurements, the ■ stands for the prior statistical distribution from an information theoretical analysis. The insert is the expanded portion of $v'' = 3$–7. ○ is the experimental data and □ is the predicted distribution from the Franck–Condon/golden rule model (see text).

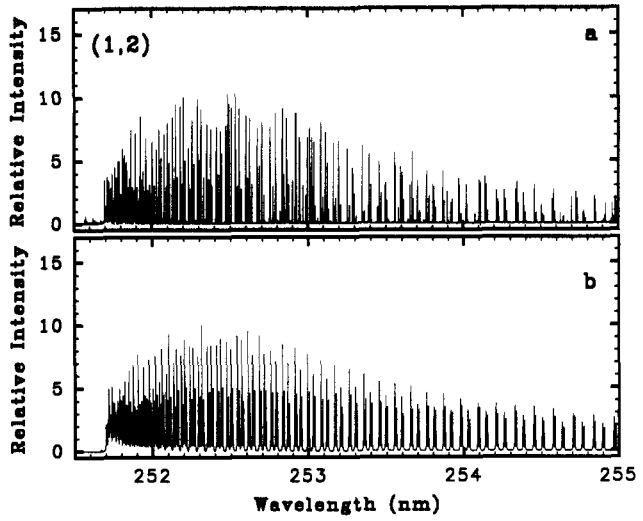

Figure 5. (a) Laser induced fluorescence excitation spectrum of the (1, 2) band of the $SO(B^3\Sigma^-–X^3\Sigma^-)$ transition following the photolysis of 0.020 Torr Cl_2SO at 193 nm. A probe delay of 400 ns was used. (b) Simulated spectrum, assuming a Boltzmann rotational state distribution (T_{rot} = 1400 K) and a Gaussian spectral line profile (FWHM = 0.25 cm^{-1}). For more information on simulation parameters, see text.

transition frequencies based on Colin's spectroscopic constants.[19] These experimental spectra were calibrated by adjusting the bandheads to the literature values. The agreement between calculated rotational line positions and the experimental positions was within 1 cm^{-1}.

The population of a single rovibrational state $P(v'', N'')$ is related to the observed intensity of the LIF rovibronic transition, $I(v', N' - v'', N'')$, by[22]

$$P(v'', N'') = I(v', N' - v'', N'')\cdot g(J'')/S(N', N'') \quad (5)$$

where $S(N', N'')$ is the Hönl–London factor[24] and $g(J'')$ is the rotational degeneracy, $(2J'' + 1)$. The nascent rotational-state population for the vibrational bands of $(1, n)$, where n = 1–3, could be directly obtained from P_{22} and/or R_{22} (*cf.* Figure 6), because these two branches are nearly resolved for the higher rotational levels, $N > 10$. By mapping our observed rotational-state distribution on a Boltzmann plot, *i.e.*, $\ln[P/g(J'')]$ vs $E_r(N'')$, we can obtain a linear least squares fit, with a slope of

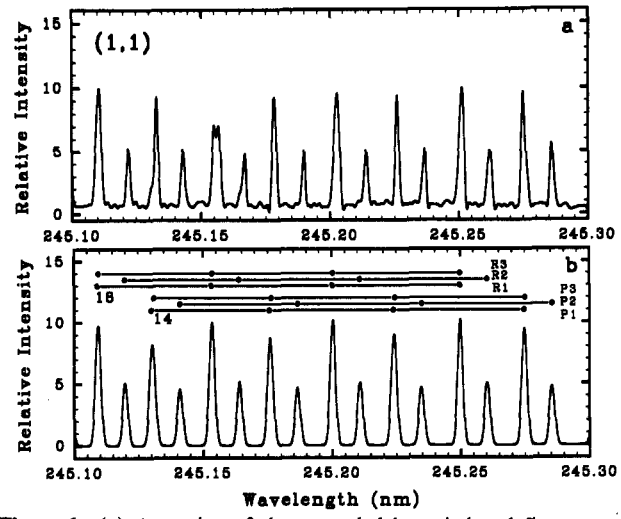

Figure 6. (a) A portion of the expanded laser induced fluorescence spectrum of the (1, 1) band of the SO(B–X) transition following the photolysis of 0.020 Torr Cl_2SO at 193 nm. The probe delay of 400 ns was used. (b) Simulated spectrum assuming a Boltzmann rotational state distribution (T_{rot} = 1800 K) and a Gaussian spectral line profile (FWHM = 0.25 cm^{-1}).

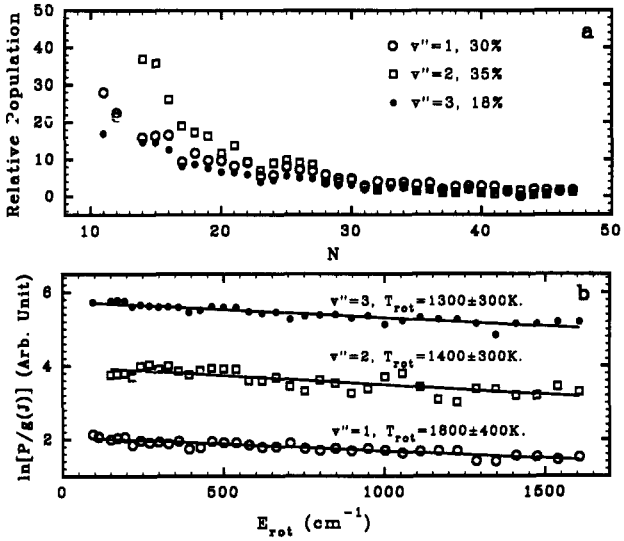

Figure 7. (a) Nascent rotational state distributions of the SO(X, $v'' =$ 1–3) measured at 400 ns following the 193-nm photodissociation of 0.020 Torr Cl_2SO. (b) Semilog plot of relative population in the rotational levels of the $SO(X^3\Sigma^-, v'')$ state, corrected to the rotational degeneracy, $g(N'') = (2N'' + 1)$, versus the rotational energy, E_{rot}. The solid lines are linear least square fits to the data in the vibrational states of $SO(X^3\Sigma^-$, $v'' = 1$–3), and each corresponds to a Boltzmann temperature (see text).

$-1/kT_{rot}$, from which rotational temperatures, T_{rot}, for the nascent $SO(X^3\Sigma^-)$ result. All the observed rotational-state distributions for the nascent SO(X, $v'' = 1$–3) from the photodissociation of Cl_2SO at 193 nm can be described by a Boltzmann distribution (Figure 7). The rotational temperatures of the nascent $SO(X^3\Sigma^-)$ for $v'' = 1$–3 were obtained and listed as follows:

v''	1	2	3
T_{rot}	1800 ± 400 K	1400 ± 300 K	1300 ± 300 K

The rotational-state population of the nascent $SO(X^3\Sigma^-)$ in the lower rotational levels, *i.e.*, $N < 10$, cannot be obtained directly from the spectrum because the corresponding spectral lines were not resolved. This problem was addressed by spectral simulation. A Boltzmann rotational-state distribution with a trial temperature and a Gaussian profile (FWHM = 0.25 cm^{-1}) for the spectral lines were assumed to simulate the observed LIF spectra. The spectral simulation, using the temperature obtained from the Boltzmann plot of the rotational-state distribution at the higher

rotational levels yields a close resemblance to the LIF spectrum of the complete vibrational band, as shown in Figure 5.

Rotational-state distributions of SO(X, $v''=4,5$) were difficult to obtain due to strong overlap of the rovibronic lines in the (1, 4) and (1, 5) vibrational bands. The nascent rotational state distribution for $v''=0$ was also not measured because the signal-to-noise ratio was too small to give reliable data. For the photodissociation of Cl_2SO at 248 nm, no nascent rotational state population distribution for the $SO(X^3\Sigma^-)$ has been measured because the radicals encounter *ca.* 10 gas phase collisions (20 mTorr Cl_2SO; 1 Torr He; 1 μs delay) prior to detection and the corresponding rotational state distributions were, at least partially, relaxed.

3. Spin-State Distributions of Nascent $SO(X^3\Sigma^-)$. For the nascent $SO(X^3\Sigma^-)$ resulting from the photodissociation of Cl_2SO at 193 nm, the spin-state distribution has been examined. Kanamori *et al.* found a spin polarization ratio $F_1:F_2:F_3 = 3:1:3$ for the nascent SO(X, $v''=1$) from the photodissociation of SO_2, indicating a preference for spin parallel or antiparallel vs spin perpendicular configurations.[25] In our experiments, we can resolve F_1, F_2, and F_3 at high N (>30) levels but cannot resolve F_1 and F_3 for $10 \leq N < 30$. For $N = 30$–47, we found $F_1 = F_3$ and therefore assumed $F_1 = F_3$ for $N = 10$–30, where the two components cannot be resolved. The population in F_2 was directly obtained from resolved spectral lines, which allows us to compare the spin states $F_1 = F_3$ vs F_2. As an example, the result for $SO(X^3\Sigma^-, v''=1)$ is shown as Figure 8. Unlike in the case of SO_2,[25] the ratios for the nascent spin-state distribution, F_1/F_2, were found to be close to unity. For $v''=2$, the spin-state distribution could be similarly obtained. For $v''=3$–5, however, because of the overlap of the rovibronic transitions with different rotational quantum numbers, the ratios can only be obtained approximately by comparing the intensities of the spectral peaks containing F_1 and F_3 with those containing F_2 and normalizing them to the Hönl–London factors. These spin-state distribution ratios (F_1/F_2) were averaged over all the rotational states in single vibrational levels. The F_1/F_2 ratios obtained for the nascent $SO(X^3\Sigma^-)$ from photolysis of Cl_2SO at 193 nm have been found to be 1.0 ± 0.4 for $v''=1$; 1.1 ± 0.3 for $v''=2$; 0.9 ± 0.4 for $v''=3$; 0.9 ± 0.4 for $v''=4$ and 1.2 ± 0.5 for $v''=5$ (errors are 2σ). The spin-state distribution ratio cannot be measured in the vibrational state of $v''=0$ because the signal-to-noise ratio is too small to give a reliable result. In the case of the photodissociation of Cl_2SO at 248 nm, no spin-state distribution for $SO(X^3\Sigma^-)$ was measured since the SO radical produced was no longer nascent (0.020 Torr Cl_2SO; 1 Torr He; and 1 μs delay) and the spin-state distribution could be relaxed.

4. Quantum Yield of Nascent $SO(X^3\Sigma^-)$. The measurement of the quantum yield of $SO(X^3\Sigma^-)$ production may provide insight into the photodissociation mechanism of Cl_2SO, particularly in light of the fact that other electronic states of SO are energetically allowed. In our experiments, the LIF signal of a given rovibronic transition corresponding to $SO(X^3\Sigma^-, v''=1)$ vibrational state was used to measure the quantum yield. We use $v''=1$ because this is the state where there is significant nascent population for the case of the photodissociation of Cl_2SO at both 193 and 248 nm and for the photodissociation of SO_2 at 193 nm as well. The LIF signal intensity was found to be linear with respect to the concentration of $SO(X^3\Sigma^-)$ radical by varying the pressure of sample gas, Cl_2SO or SO_2, around 0.020 Torr. One Torr of helium was added as buffer gas, and a 2 μs delay between the photolysis and probe lasers was used to insure the rotational- and spin-state relaxation. We recorded the LIF signal intensities originating from $SO(X^3\Sigma^-)$ from the photodissociating Cl_2SO and SO_2, respectively, under identical conditions except for photolysis laser fluence (25 mJ/cm^2 at 193 nm and 65 mJ/cm^2 at 248 nm). The LIF signal intensity was the average of 2000 points, and the data we used for the quantum yield calculation was the average of 10 signals. The quantum yield, ψ, of the $SO(X^3\Sigma^-)$ was derived as follows:

$$\psi \propto I_{SO(I)}/[\sigma \cdot P(v'') \cdot P_{Laser}] \qquad (6)$$

where the σ is the absorption cross section of the parent molecule at the corresponding photolysis wavelength, $P(v'')$ is the fractional nascent population in the vibrational state of $SO(X^3\Sigma^-, v''=1)$, and P_{Laser} is the fluence of the photolysis laser. Because the $SO(X^3\Sigma^-)$ production is greater than 99.5% from the photolysis of SO_2 at 193 nm,[15] we assume it to be unity. By comparing ψ value from the photolysis of Cl_2SO at both 193 and 248 nm with the ψ value from the photolysis of SO_2 at 193 nm, relative quantum yield, Φ, of $SO(X^3\Sigma^-)$ from Cl_2SO were obtained.

$$\Phi_{193nm}^{Cl_2SO} = \psi_{193nm}^{Cl_2SO}/\psi_{193nm}^{SO_2} = 0.73 \pm 0.10$$

$$\Phi_{248nm}^{Cl_2SO} = \psi_{248nm}^{Cl_2SO}/\psi_{193nm}^{SO_2} = 0.13 \pm 0.07$$

The errors are statistical, based on the multiple measurements. The large error of the quantum yield measurement in the case of 248-nm photolysis most likely arises from the change of the photolysis laser source and/or the change of the related optical components.

Discussion

1. 193-nm Photodissociation. According to Strauss and Houston,[5] a concerted dissociation is defined as one in which all the bond-breaking events occur on a time scale shorter than a rotational period of the possible reaction intermediate, which, in turn, allows anisotropic effects to be observed experimentally. By measuring the internal state distributions of the fragment(s), information about whether or not a photodissociation process occurs in concert may be directly revealed. For example, in a concerted process, the vibrational-state distributions of the fragment(s) may reflect characteristics of the Franck–Condon excitation, since the final state interactions are weak due to the rapid cleavage of all the bonds. In this case, the distribution of the fragment(s) may be inverted or nonstatistical, while in a stepwise dissociation, a thermalized distribution of the product states may be expected since a long-lived intermediate may allow the statistical distribution and/or disposal of the excess energy.

In our experiments, rotational-state distributions of the nascent SO can be characterized by a single temperature, suggesting that there is one major dissociation channel responsible for the production of ground-state sulfur monoxide. The uniform spin-state distributions ($F_1/F_2 = 0.9$–1.2 error = ± 0.4) for $SO(X^3\Sigma^-$, $v''=1$–5) are also consistent with this hypothesis. The inverted vibrational distribution of $SO(X^3\Sigma^-)$ that results from the Cl_2SO dissociation indicates that both Cl–S bonds break within a short enough time so as to minimize final state interactions. Since no spectroscopic data are available for OSCl, the rotational period is taken as 3×10^{-12} s assuming the rotational constant $B = 1$ cm^{-1} (typical order for nonlinear triatomic molecules) and $N \sim 10$. The vibrational periods of OSCl, corresponding to the three vibrational modes, are estimated from the data available for SSCl to approximate the possible intermediate in our experiment.[26] These vibrational periods are estimated to be 5×10^{-14}, 5.6×10^{-14}, and 9.8×10^{-14} s, respectively. The order of these time scales are assumed to be true for OSCl. From this estimate, the intermediate, OSCl, would vibrate over 50 times in one rotational period. In the case that the nascent $SO(X^3\Sigma^-)$ was produced via a stable OSCl intermediate that lives longer than a rotational period, the intramolecular vibrational energy randomization during the lifetime of the intermediate would produce a thermalized, *i.e* noninverted, distribution. Thus the existence of a stable OSCl intermediate is not likely in the photochemical pathway for the production of nascent $SO(X^3\Sigma^-)$ following irradiation at 193 nm. The major channel, which produces the nascent $SO(X^3\Sigma^-)$ in the photodissociation of Cl_2SO at 193

TABLE III: Energy Disposal into Different Degrees of Freedom of the Nascent SO Photofragment Following 193-nm Photodissociation of Cl_2SO Assuming a Concerted three-Body Dissociation[b]

mode	this work	previous work[a]
E_{vib}^{SO}	7.2	
E_{rot}^{SO}	3.1	
E_{trans}^{SO}	<11	
E_{trans}^{SO+2Cl}	<28	26
E_{total}	<38.3	

[a] Reference 8. [b] The available energy is 39.7 kcal/mol.

nm, most likely proceeds via a concerted dissociation mechanism in which one S–Cl bond may break first, but the second one must cleave within one rotational period of the assumed reaction intermediate, OSCl.

To further address the major dissociation channel, the energy disposal into the fragments was analyzed. The energy disposal into the vibrational degree of freedom of the $SO(X^3\Sigma^-)$ fragment was evaluated as the sum of the energy partitioned into each vibrational level: $E_{vib} = \Sigma c_v(E_v - E_o)$, where c_v is the fractional population in v'' state obtained from Figure 3, and E_v and E_o are the energy of the given vibrational level v'' and the zero point energy of the electronic state, respectively. The average vibrational energy, E_{vib}, for $SO(X^3\Sigma^-)$ from the photodissociation of Cl_2SO at 193 nm was calculated to be 7.2 ± 1.2 kcal/mol. The rotational energy at each vibrational level was estimated by $E_r(v'') = kT_r(v'')$, where T_{rot} is the rotational temperature in the given vibrational state, and the other variables are the same as given above. The average rotational energy, E_{rot}, for the $SO(X^3\Sigma^-)$ was estimated by $\Sigma(K_B T_{rot} \cdot c_v)/\Sigma c_v$ and calculated to be 3.1 ± 0.9 kcal/mol. The average internal energy disposal into the nascent $SO(X^3\Sigma^-)$ was found to be 10.3 ± 2.1 kcal/mol.

The upper limit of the translational energy of the nascent $SO(X^3\Sigma^-)$ fragment was found to be 11 ± 2 kcal/mol by assuming that the observed spectral line width of a single rovibronic transition is its Doppler width. This assumption is at best an upper limit since the observed spectral line widths are close to the probe laser bandwidth. The average translational energy can be calculated based on the kinetic energy of the nascent $SO(X^3\Sigma^-)$. Assuming three-body dissociation geometry, the following equations were used to calculate the total kinetic energy

$$m_{SO} \cdot v_{SO} = 2m_{Cl} \cdot v_{Cl} \cdot \cos(a/2) \quad (7)$$

$$E_{trans}^{SO+2Cl} = {}^1/_2 \cdot (m_{SO} \cdot v_{SO}^2 + 2m_{Cl} \cdot v_{Cl}^2) \quad (8)$$

where m represents the mass, v is the velocity, and a is the angle of Cl–S–Cl (~97°).[31] Based on these equations, $v_{Cl} = 1.03 \cdot v_{SO}$ and $E_{trans}^{SO+2Cl} = 2.56 \cdot E_{trans}^{SO}$ were obtained. The calculation yields an upper limit value of $E_{trans}^{SO+2Cl} < 28$ kcal/mol. This value is consistent with the result of Baum *et al.* of 26 ± 3 kcal/mol (peak value) for the photofragment translational energy of SO + 2Cl following 193-nm photolysis of Cl_2SO.[8] It is important to note that if the two chlorine atoms dissociate in sequential steps, but in less than a rotational period of ClSO, then the average translational energy release to the photofragments can be either greater than or less than the value obtained here, depending on the dynamics of each of the processes. The overall energy disposal into the various modes of the nascent fragments is summarized in Table III.

The total energy disposal into the three fragments $SO(X^3\Sigma^-)$ + 2Cl is found to be 38.3 ± 5 kcal/mol if a three-body dissociation is assumed, and $E_{trans}^{SO+2Cl} = 28$ kcal/mol (upper limit) was used. This value is in close agreement with the total available energy of 39.7 kcal/mol for $Cl_2SO + h\nu \rightarrow SO(X^3\Sigma^-) + Cl + Cl$ at 193 nm.[8] This energy balance analysis supports our hypothesis that the SO in its ground state, $X^3\Sigma^-$, is most likely produced via a concerted three-body dissociation (3). The production yield of the nascent $SO(X^3\Sigma^-)$ from the 193-nm photolysis of Cl_2SO, which was found to be 73 ± 10% in our experiments, is consistent with Baum *et al.*'s conclusion of 80% proceeding by the three-body dissociation (3).[8] These results suggest that most of the nascent $SO(X^3\Sigma^-)$ population following the 193-nm irradiation on Cl_2SO must be produced via the concerted three-body dissociation channel (3) rather than the molecular elimination of Cl_2 (2).

We have concluded thus far that the concerted three-body fragmentation, $Cl_2SO \rightarrow SO + Cl + Cl$, is the major dissociation channel for Cl_2SO photolysis at 193 nm to produce $SO(X^3\Sigma^-)$. This raises the question, Does the dissociation take place on the potential surface of an initially excited repulsive state or is it a predissociation where the molecule crosses from a bound excited state potential to a repulsive surface?[2] Modeling the nascent vibrational distribution may be useful in providing insight into this question, if we can predict the Cl_2SO geometry immediately prior to dissociation.[7,27]

Several research groups have applied a Franck–Condon/golden rule treatment to model inverted vibrational distributions of nascent products from elementary chemical reactions.[7,27-30] This model assumes a sudden transition from the "dressed" precursor, *e.g.*, AB in the parent molecule ABCD, to the "undressed" diatomic photofragment and calculates the probability, $P(f)$ of forming nascent AB in vibrational state, $|f\rangle$

$$P(f) \sim (4\pi^2/h)|\langle i|f\rangle|^2 \rho(E) \quad (9)$$

where $|i\rangle$ is the initial "dressed oscillator" state, corresponding to SO in the parent molecule, *e.g.*, SO in Cl_2SO, $\rho(E)$ is the density of the final states, and h is Planck's constant. Morse oscillator functions are used for $|f\rangle$ and $|i\rangle$. Application of this model to the photofragmentation of Cl_2SO at 193 nm reveals the bond length for the "dressed" S=O moiety prior to the dissociation of this tetratomic molecule. Unlike in the case of SO_2,[7] the S=O bond length in the ground-state Cl_2SO (d_{SO} = 1.44 Å)[31] with a trial vibrational frequency of 1200 cm^{-1} leads to close agreement with the LIF measured SO vibrational distribution, as shown in Figure 3. This result suggests a direct dissociation mechanism, *i.e.*, excitation of the ground state to a repulsive state, may be operative. A direct dissociation is consistent with the following: (i) our observation of unity spin-state distribution ratios are consistent with a direct dissociation mechanism where no potential surface crossing, which may produce spin polarization,[25] is operative; (ii) the Cl_2SO absorption band near 193 nm is assigned to $n_{Cl} \rightarrow \sigma^*_{S-Cl}$[6,10] which may lead to an immediate rupture of both S–Cl bonds; (iii) the hypothesis is also consistent with the Baum *et al.* claim that the anisotropy of all the fragments from the photodissociation of Cl_2SO at 193 nm could be accommodated by one initially excited state of A″ symmetry.[8] On the other hand, if a predissociation via an excited state with a *different* SO bond length was assumed, then d_{SO} = 1.61 Å and v = 1100 cm^{-1} would be required to fit our LIF observation. Such a significant (12%) elongation of the S=O bond is not likely since the $n_S \rightarrow \pi_{SO}^*$ transition which could lead to the elongation of the S=O bond is far to the red of 193 nm ($\lambda > 250$ nm[6]). A small difference between the observed and predicted distributions exists and may suggest the involvement of final state interactions. Further investigation, especially the rotational state distribution dependence on the initial thermal conditions of the parent molecule,[32] is needed to clarify whether the Cl_2SO dissociation is direct or indirect.

Besides the major dissociation channel, there may be some minor photochemical pathways which are also responsible for the production of nascent SO in the photodissociation of Cl_2SO at 193 nm. One could be the secondary dissociation of the OSCl intermediate, while another could be the molecular elimination channel (2).[8] Folllowing the radical elimination channel, a further cracking of OSCl into SO and Cl is possible, either via a

unimolecular decay or via a secondary photodissociation. The latter is ruled out in the experiments of Baum *et al.*[8] Much lower photolysis laser fluences are used in our experiments (0.25 mJ/mm^2) in comparison with theirs (700 mJ/mm^2), which allows us to also rule out such a possibility. Furthermore, our observed signal intensities are linear with respect to photolysis laser fluence. Since we observe an inverted vibrational distribution with almost no nascent population in $v'' = 0$, it is not likely that the OSCl thermal decay contributes significantly. Baum *et al.* report that as much as 17% of the photoactivated Cl_2SO dissociates via elimination of Cl to produce OSCl.[8] Decay of this OSCl should yield an observable population in the $v'' = 0$ state, since most of the $SO(X^3\Sigma^-)$ produced by OSCl decay would be expected to produce the ground vibrational state. For the photodissociation of dimethyl sulfoxide (DMSO) at 193 nm, 14% of the nascent $SO(X^3\Sigma^-)$ population is found in the vibrational ground state under similar photolysis conditions, which serves as an indicator of the LIF measurability of SO(X, $v'' = 0$).[33] No nascent population was measured for $v'' = 0$ in the photodissociation of Cl_2SO at 193 nm, even when the (2,0) and (3,0) transitions were used to probe the ground state. The Franck–Condon factors for these transitions are reported to be 4–10 times larger than for the (1,0) transition.[20] We estimate that less than 5% of the nascent $SO(X^3\Sigma^-)$ produced in the 193-nm photolysis of Cl_2SO has population in $v'' = 0$, by comparison with the signal of the same bands following the photolysis of DMSO at 193 nm.[33]

The molecular elimination channel may produce $SO(X^3\Sigma^-) + Cl_2(B^3\Pi^+)$, which is allowed under spin selection rules,[8,34] and has been studied by Baum *et al.* to have a quantum yield of 3%.[8] Following the molecular elimination, Cl_2 may undergo further dissociation to yield Cl + Cl. However, no electronically predissociative states of Cl_2 in the accessible energy range are available, and tunnelling the centrifugal barrier of a rotational metastable state is not likely for chlorine due to its large reduced mass.[8] Therefore, besides the primary three-body dissociation, the most likely production chemical for $SO(X^3\Sigma^-)$ is molecular elimination of Cl_2.[8]

Our experiments still fail to account for the fate of all the photoactivated Cl_2SO. Baum *et al.* found direct evidence for the presence of OSCl ($m/e = 83$) following 193-nm photolysis of Cl_2SO, most of which they believed to be in an electronically excited state. Another possibility is that this discrepancy could be ascribed to the production of nascent SO in other electronic states, such as a $^1\Delta$ state, investigated by Kanamori *et al.* with an infrared diode laser,[15] or the $b^1\Sigma$ state. Further studies are still needed to clarify this issue.

2. 248-nm Photodissociation. Photodissociation of Cl_2SO at 248 nm can proceed energetically along the same three pathways as at 193 nm, but Baum *et al.* claim that only the molecular elimination of Cl_2 (2) and/or the radical elimination of OSCl (1) are operative.[8] No further fragmentation of OSCl, deriving from the initial photoactivation, was found in their experiments. However, nascent $SO(X^3\Sigma^-)$ has been observed in our experiments for the same photodissociation and is produced with a bimodal vibrational distribution. The production yield for the total nascent $SO(X^3\Sigma^-)$ has been measured as 13 ± 7% in this case, and the first three vibrational levels ($v'' = 0$–2) accounted for 94% of the nascent $SO(X^3\Sigma^-)$ population. The nascent $SO(X^3\Sigma^-, v'' = 0$–2) was found to observe a Boltzmann distribution, suggesting a stepwise mechanism involving the unimolecular decay of OSCl into SO and Cl. The vibrational temperature of the nascent $SO(X^3\Sigma^-)$ for $v'' = 0$–2 has been found to be T_{vib} 1000 ± 200 K. To further characterize the dissociation mechanism, the experimental data were fit to a prior distribution calculated by an information theoretical model, in which the total energy conservation is considered and the conservation of angular momentum is neglected.[35–37] The pure statistical expectation for the nascent vibrational distribution for a chemical reaction involving AB + C has been formulated as follows[35]

$$P^o(v'|E_{tot}) = (E_{tot} - E_{v''})^{3/2} / \sum (E_{tot} - E_{v''})^{3/2} \quad (10)$$

where E_{tot} is the operative excess energy (set as a trial variable) in the spontaneous dissociation of $OSCl \rightarrow SO(X^3\Sigma^-) + Cl$, $E_{v''}$ is the vibrational energy corresponding to the individual vibrational levels, and $P^o(v'|E_{tot})$ stands for the prior expectation for the vibrational population. The observed vibrational distribution was fit by a calculated distribution from the above model by varying E_{tot}. The excess energy, $E_{tot} = 9.1$ kcal/mol, was found to give the best fit of the data (see Figure 4), $v'' = 0$–2, which is in close agreement with the excess energy (7 kcal/mol) for the process: $Cl_2SO + h\nu$ (248 nm) $\rightarrow SO + Cl + Cl$.[8] The small difference between the fit value and the thermodynamic data may correspond to the contribution of the zero-point energy prior to the secondary fragmentation. Higher excess energy, E_{tot}, can lead to population in the higher vibrational states, *e.g.*, $v'' = 3$. However, no calculated distribution containing population in $v'' = 3$ was found in close agreement with our observed LIF data, indicating $E_{tot} = 9.1$ kcal/mol is the best fit excess energy. The nascent population in the vibrational levels of $v'' = 3$ and higher are not likely to be produced via the unimolecular fragmentation of the OSCl intermediate.

The information content is defined as[35]

$$I = \Sigma - P(v'|E_{tot}) \cdot \ln[P(v'|E_{tot})/P^o(v'|E_{tot})] \quad (11)$$

which serves as a direct measure about the deviation of the observed vibrational distribution, $P(v'|E_{tot})$, from the statistical prior expectation, $P^o(v'|E_{tot})$. In the limiting case, where the observed distribution matches the prior expectation in all the vibrational states, the information content, I, should be zero.[35] Otherwise, it is a positive value which implies deviations from a pure statistical character. The value of I has been found to be 0.04 ± 0.02 from our observed data, which indicates a small deviation from a statistical distribution determined purely from the principle of maximum entropy. Thus, the unimolecular fragmentation of OSCl is believed to be responsible for the production of the nascent SO(X, $v'' = 0$–2) in the photodissociation of Cl_2SO at 248 nm. The average vibrational energy in the SO(X, $v'' = 0$–2), which is 2.6 ± 0.5 kcal/mol according to our LIF measurements, accounts for 29% of the total excess energy of $E_{tot} = 9.1$ kcal/mol, again in close agreement to the prediction ($E_{tot}/3$) by a pure statistical vibrational energy disposal model in the OSCl intermediate.[37] The different mechanisms for the primary dissociation channels, which produce $SO(X^3\Sigma^-)$, in the laser photolysis of Cl_2SO at 193 and 248 nm are summarized in Figure 9.

The nascent population in the $SO(X^3\Sigma^-, v'' = 3$–7) in the photolysis of Cl_2SO at 248 nm cannot be produced energetically via a three-body fragmentation, either concerted or sequential. Photodissociation involving a multiphoton process was ruled out because the LIF signal of the SO(B, 1-X, v') transitions, *e.g.*, for $v'' = 4$ and 5, were found to be linear with respect to the photolysis laser fluence. The nascent population in $SO(X^3\Sigma^-)$ for $v'' = 3$–7 is most likely produced by the molecular elimination of Cl_2 from Cl_2SO since it is the only energetically allowed (single 248-nm photon) channel for the production of the nascent population in these vibrational states. The 248-nm photolysis provides a good source for the investigation of the molecular elimination channel (2) in the dissociation of Cl_2SO. In the photolysis at 193 nm, the minor molecular elimination channel (2) has been obscured by the primary three-body dissociation process (1), since both seem to produce inverted vibrational distributions. At 248 nm, the stepwise dissociation process dominates the $SO(X^3\Sigma^-)$ production, but it is separated, by the nascent vibrational levels produced, from the molecular elimination channel (2). The stepwise channel can only populate the $SO(X^3\Sigma^-)$ up to $v'' = 2$. The rest of the

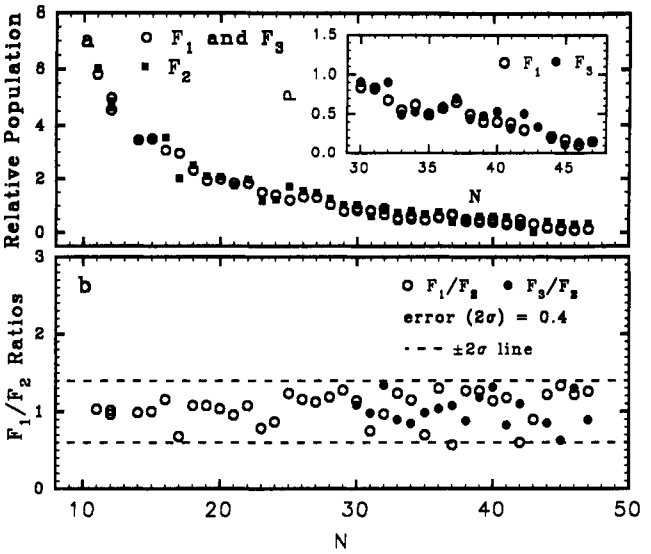

Figure 8. (a) Nascent rotational state distributions of the $SO(X^3\Sigma^-, v'')$ measured at 400 ns following the 193-nm photodissociation of 0.020 Torr Cl_2SO. O represents the population in the spin state F_1 or the average in both F_1 and F_3 when the two states cannot be resolved in the region of N = 10–30. The insert shows the comparison of the population in F_1 (O) and F_3 (●) states. (b) The spin state distribution ratio of F_1/F_2 for $SO(X^3\Sigma^-, v''=1\text{–}3)$. The dashed line, – –, represents the error (2σ). The averaged F_1/F_2 ratio is found to be 1.0 ● 0.4 for v'' = 1.

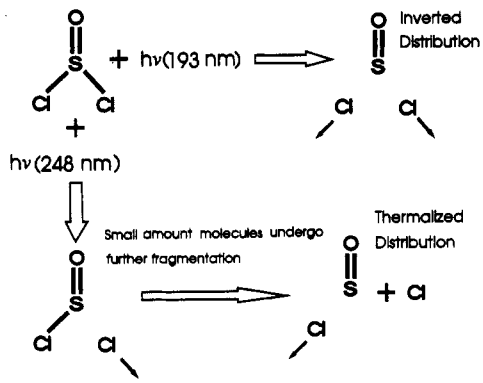

Figure 9. A schematic diagram showing the different primary dissociation mechanisms for the photodissociation of Cl_2SO at 193 and at 248 nm.

vibrational levels, v'' = 3–7, provide a clean $SO(X^3\Sigma^-)$ source for the investigation of the molecular elimination channel (2). Baum *et al.* found a 3.5% quantum yield for this molecular elimination channel and a 9:1 branching ratio for the $b^1\Sigma^+$ and $X^3\Sigma^-$ states,[8] respectively, thus giving a small quantum yield of 0.35% for the production of the $SO(X^3\Sigma^-)$ via this process (channel 2). Our LIF quantum yield observation of less than 1% for the total nascent population of $SO(X^3\Sigma^-)$ in the v'' = 3–7 levels is consistent with their observation.

Even though the total population for this photochemical channel is small, the nascent vibrational distribution of $SO(X^3\Sigma^-, v'' = 3\text{–}7)$ was found to be inverted with a population maximum at v'' = 5. The inverted vibrational distribution indicates a fast process, which is consistent with the nature of the molecular elimination of Cl_2.[8] The Franck–Condon/golden rule model (see above) using an S=O bond length consistent with ground-state Cl_2SO (1.44 Å)[31] cannot rationalize an inverted vibrational distribution peaked at v'' = 5, suggesting an indirect dissociation. In order to obtain a calculated vibrational distribution to fit our data (see the insert plot of Figure 4), an elongated S=O bond length of about 1.8 Å was required. This may be consistent with the partial overlap between the transition of $n_S \rightarrow \pi_{SO}^*$ ($\lambda > 250$ nm[6]) and the laser radiation at 248 nm, and, thus, photoactivation of Cl_2SO may produce significant elongation of the S=O bond via the $n_S \rightarrow \pi_{SO}^*$ transition. A second possibility is the dissociation of the highly vibrationally excited ground electronic state Cl_2SO following internal conversion from the initially prepared state.

The average vibrational energy of the SO fragment via the molecular elimination of Cl_2 was calculated to be 15.5 kcal/mol by using the same procedure as for the case of the photolysis at 193 nm, assuming that no population in the vibrational levels of v'' = 0–2 was produced from channel (2). The nascent rotational state distributions of the SO fragment were not probed directly, but we assume the results of E_{rot} = 3.1 kcal/mol from the 193-nm case as an estimate. The total translational energy for SO + Cl_2 was taken from the peak value (24 kcal/mol) of ref 8. The only energetically allowed state of Cl_2 is the ground state, $X^1\Sigma^+$.[8,39] An energy balance analysis leaves 21.3 kcal/mol to be disposed into the internal states of the nascent Cl_2. This large amount of internal energy into Cl_2 is consistent with the large change in Cl–Cl distance in going from Cl_2SO (3.09 Å)[31] to Cl_2 (2.44 Å)[39] via a three-center transition state. Consequently, significant vibrational excitation may result from the formation of the Cl–Cl bond in the 248-nm photodissociation of Cl_2SO.

Summary and Conclusions

Following the 193-nm photodissociation of Cl_2SO, the nascent vibrational state distribution of $SO(X^3\Sigma^-, v'' = 0\text{–}6)$ is found to be inverted with a population maximum at v'' = 2 by using laser induced fluorescence (LIF) spectroscopy of $SO(B^3\Sigma^- – X^3\Sigma^-)$ in the region of 237–295 nm. The nascent rotational state distributions of $SO(X^3\Sigma^-)$ for v'' = 1, 2, and 3 have been obtained and can be characterized by a single temperature distribution. The spin-state distributions have been found to be unpolarized (F_1/F_2 = 0.9–1.2 error = ±0.4) for all the vibrational states measured. The primary quantum yield for the production of $SO(X^3\Sigma^-)$ was measured to be $\Phi_{SO(X)}^{193nm} = 0.73 \pm 0.10$. The single temperature rotational-state distributions and uniform spin-state distributions suggest that one primary dissociation channel is responsible for the nascent $SO(X^3\Sigma^-)$. The inverted vibrational-state distribution of the nascent $SO(X^3\Sigma^-)$ fragment indicates that this dissociation channel is a concerted process in which both S–Cl bonds cleave within *ca.* 10^{-12} s. Quantum yield measurements and an energy disposal analysis support the concerted three-body fragmentation to produce SO + Cl + Cl, as the major dissociation channel. A Franck–Condon/golden rule model elucidates the dissociation geometry as similar with the equilibrium structure of the ground-state Cl_2SO, suggesting a direct dissociation. The unity spin-state distribution ratios are also consistent with a direct dissociation mechanism. Other minor dissociation channels, such as molecular elimination of Cl_2 and the production of SO in electronic states other than $X^3\Sigma^-$ cannot be ruled out.

Photolysis of Cl_2SO at 248 nm produces a nascent vibrational-state distribution of $SO(X^3\Sigma^-)$ that is characterized as bimodal. The data are consistent with production of $SO(X^3\Sigma^-)$ by two different processes, a stepwise fragmentation of the S–Cl bonds and a molecular elimination of Cl_2 via a three-center transition state. The two channels are well-separated in the production of the nascent $SO(X^3\Sigma^-, v'')$ in different vibrational levels (v'').

The detailed results described here have provided valuable insight into the nature of multiple bond photofragmentation processes. The two wavelengths employed delineate distinct photochemical behaviors and are suggestive of possible state-selective behavior. Future studies aimed at exploring the wavelength region in between those used here, may provide crucial information toward a greater understanding of multiple bond photofragmentation. These experiments are ongoing in our laboratory.

Acknowledgment. The experiments performed here were done in conjunction with the Puerto Rico Laser and Spectroscopy Facility at the University of Puerto Rico, under the auspices of the NSF-EPSCoR Program. We would also like to kindly

acknowledge the Air Force Office of Scientific Research (Grants F49620-92-5-0406 and F49620-93-1-0110) which has generously supported this research.

References and Notes

(1) Rosker, M. J.; Dantus, M.; Zewail, A. H. *J. Chem. Phys.* **1988**, *89*, 6113–6128.
(2) Schinke, R. *Comm. At. Mol. Phys.* **1989**, *23*, 15.
(3) Trentelman, K. A.; Kable, S. H.; Moss, D. B.; Houston, P. L. *J. Chem. Phys.* **1989**, *91*, 7498.
(4) Borden, W. T.; Loncharich, R. J.; Houk, K. N. *Annu. Rev. Phys. Chem.* **1988**, *39*, 213.
(5) Strauss, C. E. M.; Houston, P. L. *J. Phys. Chem.* **1990**, *94*, 8751.
(6) Kawasaki, M.; Kasatani, K.; Sato, H.; Shinohara, H.; Nishi, N.; Ohtoshi, H.; Tanaka, I. *Chem. Phys.* **1984**, *91*, 285.
(7) Chen, X.; Asmar, F.; Wang, H.; Weiner, B. R. *J. Phys. Chem.* **1991**, *95*, 6415.
(8) Baum, G.; Effenhauser, C. S.; Felder, P.; Huber, J. R. *J. Phys. Chem.* **1992**, *96*, 756.
(9) Suzuki, S.; Yamaguchi, M.; Onda, M.; Sakaizumi, T.; Ohashi, O. Yamaguchi, I. *J. Mol. Struct.* **1981**, *73*, 41.
(10) Uthman, A. P.; Demlein, P. J.; Allston, T. D.; Withiam, M. C.; McClements, M. J.; Takacs, G. A. *J. Phys. Chem.* **1978**, *82*, 2252.
(11) Yamabe, T.; Nagata, S.; Kikuzono, Y. Fukui, K. *Bull. Chem. Soc. Jpn.* **1975**, 1349.
(12) Okabe, H. *J. Am. Chem. Soc.* **1971**, *93*, 7095.
(13) Donovan, R. J.; Husain, D. Jackson, P. T. *Trans. Faraday Soc.* **1969**, *65*, 2930.
(14) Donovan, R. T. *Chemical Bonds and Bond Energies*; Academic Press: New York, 1978.
(15) Kanamori, H.; Tiemann, E.; Hirota, E. *J. Chem. Phys.* **1988**, *89*, 621.
(16) Stuart, B. C.; Cameron, S. M. and Powell, H. T. *Chem. Phys. Lett.* **1992**, *191*, 273.
(17) Bersohn, R. In *Molecular Photodissociation Dynamics*, Ashford, M. N. R., Baggott, J. E., Eds.; Royal Society of Chemistry: London, 1987; pp 1–30.
(18) Barnhard, K. I.; Santiago, A.; He, M.; Asmar, F. Weiner, B. R. *Chem. Phys. Lett.* **1991**, *178*, 150.
(19) (a) Colin, R. *J. Chem. Soc., Faraday Trans.* 2 **1982**, *78*, 1139. (b) Colin, R. *Can. J. Phys.* **1969**, *47*, 979.
(20) Smith, W. H.; Liszt, H. S. *J. Quant. Spect. Radiat. Trans.* **1971**, *11*, 45.
(21) Gu, X.; Chen, X.; Martinez, F.; Weiner, B. R. To be published.
(22) Herzberg, G. *Molecular Spectra and Molecular Structure*, Vol. I: *Spectra of Diatomic Molecules*, 2nd ed.; Van Nostrand Reinhold: New York, 1950.
(23) Kim, R.-H. Ph.D. Dissertation, Cornell University, Ithaca, NY, 1984.
(24) Hönl-London factors for $^3\Sigma$–$^3\Sigma$ transition were calculated according to formulas; Tatum, J. B. *Can. J. Phys.* **1966**, *44*, 2944.
(25) Kanamori, H.; Butler, J. E.; Kawaguchi, K.; Yamada, C.; Hirota, E. *J. Chem. Phys.* **1985**, *83*, 611.
(26) Chiu, C. L.; Pan, S. C.; Ni, C. K. *J. Chem. Phys.* **1986**, *85*, 10.
(27) (a) Berry, M. J. *Chem. Phys. Lett.* **1974**, *29*, 323. (b) Berry, M. J. *Chem. Phys. Lett.* **1974**, *29*, 329.
(28) Berry, M. J. *Chem. Phys.* **1974**, *39*, 3114.
(29) Schatz, G. C.; Ross, J. *J. Chem. Phys.* **1977**, *66*, 1037.
(30) Mukamel, S.; Jortner, J. *J. Chem. Phys.* **1974**, *60*, 4760.
(31) Hargittai, I. In *The Chemistry of Sulphones and Sulphoxides*; Patai, S., Rappoport, Z., Stirling, C., Eds.; John Wiley & Sons: New York, 1988; pp 33–54.
(32) Andresen, P.; Ondrey, G. S.; Titze, B.; Rothe, E. W. *J. Chem. Phys.* **1984**, *80*, 2548.
(33) Chen, X.; Wang, H.; Weiner, B. R.; Hawley, M.; Nelson, H. H. *J. Phys. Chem.* see following paper, in this issue.
(34) Okabe, H. *Photochemistry of Small Molecules*; Wiley-Interscience: New York, 1978.
(35) Levine, R. D.; Bernstein, R. B. *Molecular Reaction Dynamics and Chemical Reactivity*; Oxford University Press: New York, 1987.
(36) Tamagake, K.; Setser, D. W.; Sung, J. P. *J. Chem. Phys.* **1980**, *73*, 2203.
(37) Kaplan, H. D.; Levine, R. D.; Manz, J. *Chem. Phys.* **1976**, *12*, 447.
(38) Campbell, J.; Schlag, E. W. *J. Am. Chem. Soc.* **1974**, *6*, 855.
(39) Huber, K. P.; Hertzberg, G. *Constants of Diatomic Molecules*; Van Nostrand Reinhold: New York, 1979.